Lasers in Manufacturing Conference 2021

Modeling of selective laser ablation of lithium-ion battery electrodes

Max-Jonathan Kleefoot[a,b,*] , Simon Ruck[a], Jiří Martan[b], Jens Sandherr[a],

Marius Bolsinger[a], Volker Knoblauch[a], Harald Riegel[a]

[a]*Aalen University, Beethovenstraße 1, 73430 Aalen, Germany*
[b]*University of West Bohemia, Univerzitni 8, 30100 Plzen, Czech Republic (CZ)*

Abstract

Lithium-ion batteries are an important component of the current energy and mobility transition. Various approaches are being pursued in current research regarding the production of fast chargeable electrodes. These electrode layers consist of various components that – besides the current collector – can be divided into two groups. One is the active material phase and the other is the inactive binder material phase. In addition to laser perforation, selective laser ablation to remove inactive electrode components is also being investigated in research. Within this study, a simulation model was developed that predicts the spatial temperature distribution during the laser process inside the electrode. Experimental investigations were also able to show that the active material is permanently damaged by an excessively high energy input. A comparison with the model shows good agreement here. Thus, with the help of the model, a parameter optimization can be carried out in which the active material particles are exposed but not damaged. The thereby increased active surface area promises an enhancement of the fast charging capabilities of the electrode.

Keywords: selective laser ablation; binder ablation; microstructure; thermophysical modeling; lithium-ion battery

1. Introduction

Lithium ion batteries have become increasingly important in recent years. Due to their high energy and power densities, they have advantages over conventional energy storage systems. In order to increase the fast-charging capability of highly compressed electrodes, different laser-based treatments are being followed. On the one hand, the effect of three-dimensional laser structuring is being investigated (Pfleging 2021).

* Corresponding author. Tel.: +49-7361-567-2668 .
E-mail address: max-jonathan.kleefoot@hs-aalen.de

On the other hand, the effect of selective removal of the binder material on the performance is being investigated (Ruck et al. 2019). Analyses of this using a short-pulse laser have already been carried out on the cathode and showed an increased rate capability compared to the unprocessed cathodes (Ruck et al. 2019, Bolsinger et al. 2020). By laser processing, pores on the surface that were closed by the binder during previous compaction processes can be opened again by the selective removal of the surface near binder material. As the electrode surface can reach high temperatures during this process, there is a possibility of damage to the active material particles. In order to better understand the temperature progression inside the electrode, a thermal model was built (Enderle et al. 2020), which is based on the numerical solution of the heat conduction equation (Carlslaw et al. 1948, Smith et al. 2013, Collishaw et al. 1994, Vadakkepatt et al 2016).

2. Experimental set-up

2.1. Thermal Process Modelling

The numerical solution method used in this work has already been described in detail by Enderle et al. (Enderle et al. 2020). The advantages over analytical solutions such as the Green function consist in the calculation of temperature curves with finite workpiece sizes and the absence of discontinuities (Weber et al. 2014). The model is divided into two parts. Firstly, the workpiece which consists of active material, binder, conductive additive, pores and a current collector must be defined and mathematically described. The second part is the description of the laser radiation entering the workpiece, which in this case is assumed as a constant intensity over the radius. It is used as the input signal for the heat conduction equation.

The model electrode whose surface area corresponds to the laser spot size is approximated by three ideally contacted layers. The lowest layer represents the current collector or the machine table. It also forms a heat sink with a constant temperature T0 = 20°C. Above is the porous composite of active material particles, binder and conductive additive (layer II). The porosity is considered in the volumetric considerations of this layer. The composition of layer II is defined according to the anodes used in each case in Table 1. Following the literature (Bolsinger et al. 2019, Schmidt et al.2018), this layer II is covered by a higher density binder-additive boundary layer (layer I). It is assumed that this boundary layer consists of equal mass proportions of binder and conductive additive and has no porosity. Since the existence of the top layer has not yet been investigated in the literature, this layer was set to a thickness of 1 µm.

2.2. Electrode material

For the experiments, anodes with a composition of 94 wt% graphite (SGL carbon, synthetic graphite), 2 wt% carbon black (Imerys, C-Nergy Super C65), 2 wt% 93 CMC (Nippon, Sunrose MAC 500LC) and 2 wt% SBR (Zeon, BM-451B) were used. The coated anode with an area capacity of 3 mAh/cm^3 was calendered to a density of 1.6 g/cm^3. For the investigations of the ablation thresholds, special samples of both anode phases of the electrode were produced. On the one hand, active material samples were made from compressed graphite. On the other hand, samples of pure binder phase consisting of equal parts CMC, SBR and carbon black where produced.

Table 1. Thermophysical propertied of the used electrode components

	CMC+SBR	additive	Graphite
Density ρ [kg/m³]	1295	1800	2250
Specific heat capacity c_p [J/kgK]	1505	710	710
Thermal conductivity λ [W/mK]	0.292	169	169

The thermophysical properties for the materials used are summarized in Table 1. In addition, decomposition temperatures for the binder phase of 300°C are assumed, since according to Do et al. (Do et al. 2016) the decomposition temperature of amorphous carbon begins at this point. A temperature of 700°C is assumed as the decomposition threshold for the active material, which is in crystalline form.

2.3. Laser system

The experimental investigations were carried out by using a short-pulsed TruMark5020 Yb:YAG fibre laser from TRUMPF. The laser beam with a wavelength of 1064 nm was focused on the surface of the workpiece through a scanning optic with a focal length of 160 mm. The focal diameter was about 70 µm. The investigations were performed using a pulse duration of 9 ns and a constant hatch distance of 35 µm. To investigate the influence of the laser treatment on the ablation depth and the microstructure of the sample surface, the average laser power was varied from 0.9 W to 4 W at a scanning speed of 1.5 m/s and a constant pulse repetition rate of 200 kHz, resulting in an energy input per unit length $E_{Dis} = P_{av} / v_{scan}$ of 0.6 J/m to 2.67 J/m.

A white light interferometer (WLI) NewView 8000 from ZYGO was used to perform the microstructural analysis and to determine the ablation depth. A measuring field was placed in such a way that a reference surface and a processed surface could be measured. The mean ablation depth Δz was then formed from the difference in the mean heights between the untreated reference surface and the laser treated surface. For the visual evaluation of the surface, a Leo Gemini 1525 scanning electron microscope (SEM) from ZEISS was used.

3. Results and discussion

3.1. Ablation thresholds of binder phase

In the first step, a study of the removal behavior of the binder phase is used to verify the model. For this purpose, a layer of binder phase consisting of the same parts of CMC, SBR and conductive carbon black was mixed with water and coated onto a metal plate. Line treatments with different energy inputs per unit length were performed in order to determine the removal thresholds. Figure 1 shows the results of the experimentally obtained ablation depth. It can be seen that a measurable ablation begins at a threshold energy of 0.7 J/m, for a pulse duration of 9 ns.

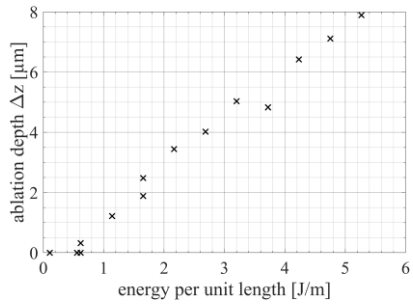

Fig. 1. Ablation depth of the binder phase at t_h = 9 ns and f_{rep} = 200 kHz

If we insert the above-mentioned material parameters into the modelling and simulate the machining of the binder phase, i.e. an anode without active material components, we get the temperature curves shown in Figure 2. As an ablation threshold energy, f 0.62 J/m is selected, because for this energy per unit length a maximum temperature of 297.42°C was reached in the interaction layer, which is just below the decomposition temperature of 300°C. This is in good agreement with the experimental results, which show a measurable removal starting at approx. 0.7 J/m. Based on a further simulation for 0.84 J/m, the decomposition threshold of the binder phase is clearly exceeded. There, the calculated temperature within the interaction layer is 394.29°C, whereupon the binder phase is removed from the electrode surface.

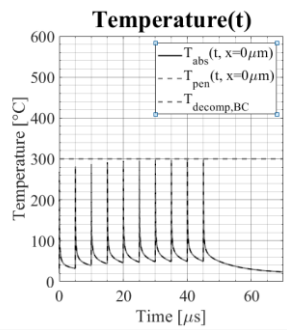

Fig. 2. Calculated temperature curves for an energy per unit length of 0.62 J/m at a pulse duration of 9 ns

3.2. Anode

In addition to the results already presented on the removal thresholds of the binder phase, the results of the entire anode model are shown in the following. The change of the surface roughness was taken into account for the evaluation. Since the objective is to remove the binder phase without removing active material, the surface roughness is due to the laser treatment distinctive for the selective removal, i.e. a change in the surface porosity. Figure 3 shows on the left ordinate the real measured change in roughness profile height of the anode as a function of the energy per unit length. The calculated depths for the evaporation of the binder

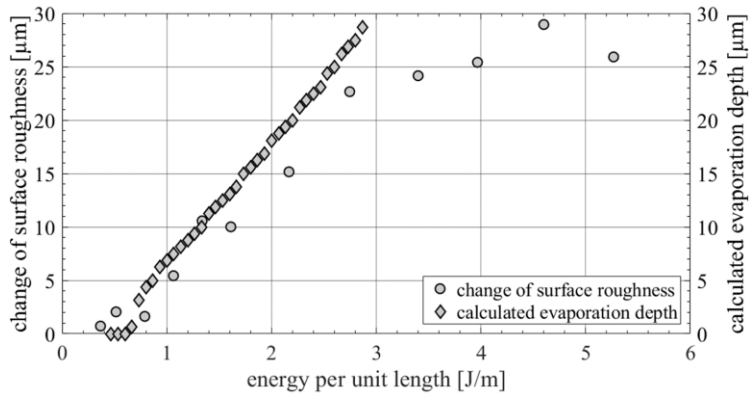

Fig. 3. Experimental results for the change of surface roughness (left ordinate) and calculated evaporation depth of the anode model (right ordinate) as function of energy per unit length for t_H = 9 ns and f_{rep} = 200 kHz

phase are shown on the right ordinate. The process thresholds of the two curves are at a comparable energy per unit length of about 0.6 - 0.7 J/m. In the lower range until approx. 2.75 J/m, the progressions of both curves are similar. Only the gradient differs slightly. This could be due to the structure of the model. In the previous model, which is constructed as a layer model similar to the experimental findings of Schmidt et al. (Schmidt et al. 2018), the integration of an attenuation constant was neglected Since a comparable layer like structure of anodes has not yet been confirmed, this may be a possible reason for the deviation. An extension of the model by a Beer-Lambert attenuation could then contribute to even better results between model and experiment.
Figure 3 also shows a bend in the experimental results above an energy per unit length of 2.75 J/m. In comparison, the modeled results continue to be almost linear. This can be ascribed with the structure of the electrode. The particle size distribution of the graphite used has a maximum in the range of about 20 µm. After removal of the entire binder on the top surface, individual particles are torn out of the surface by the vapor pressure of the evaporating binder phase below the top layer. This creates particle sized cavities in the size of a particle. Exceeding the decomposition temperature of graphite, which is about 700°C under ambient air, can also lead to the removal of particles.

Furthermore, three parameters were selected to show the process limitations. First, an energy per unit length of 0.62 J/m was selected (Figure 4 a), based on a temperature at the surface of 301°C calculated in the simulation. This should result in a change of the binder phase at the surface, but no depth effect is to be expected. A line energy of 1.29 J/m was selected as the next parameter (Figure 4 b), since a temperature at the surface of 553°C was calculated here, i.e. approximately in the middle between the decomposition temperatures of binder phase and active material. Here, removal of the binder to a depth of 9.36 µm can be expected without damaging the active material at the surface. The third selected parameter is an energy per unit length of 2.67 J/m (Figure 4 c). At this energy, a temperature of 1143°C is simulated at the surface, which exceeds the decomposition temperature of the active material. Therefore, it is to be expected that particles will be damaged. Based on the simulation data, processing with up to 1.6 J/m is possible without exceeding a temperature of 700°C at the surface. Thus, based on the simulation, the process window for the selective process can be set to 0.67 J/m - 1.6 J/m.

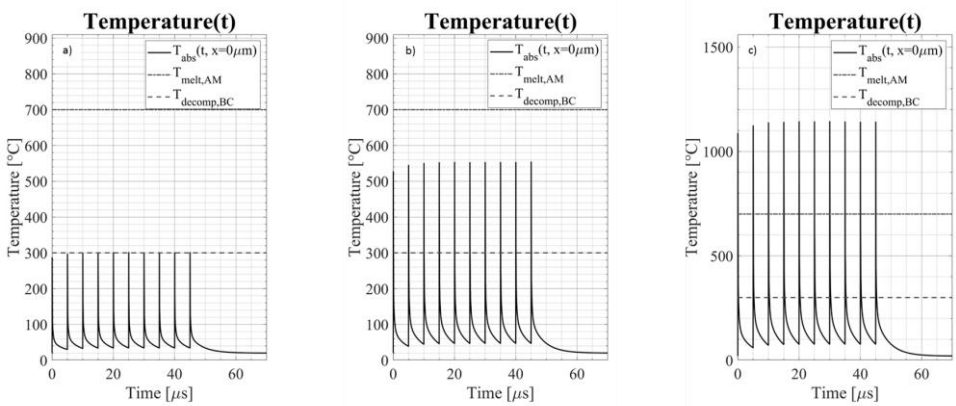

Fig. 4. Experimental results for the change of surface roughness (left ordinate) and calculated evaporation depth of the anode model (right ordinate) as function of energy per unit length for t_H = 9 ns and f_{rep} = 200 kHz

To check the assumptions from the simulation, electrodes were examined before and after processing with a scanning electron microscope. The images of this examination are shown in Figure 6. It can be clearly seen from the images that the same position and thus also the identical particles are involved in each case. Before processing (Figure 5 upper row), the surface is covered with binder. This can be seen from the curly surface structure. After processing with a line energy of 0.62 J/m (Figure 5 left column), it can be seen that there are still a few binder structures directly on the particles. However, no effect on the pore opening can be seen here. In contrast, processing with 1.29 J/m (Figure 5 middle column) shows a clear removal of the binder structures on the particles. In addition, an effect can also be seen on the particle flanks. Only in the lower left area clear binder structures can be seen within the pore. However, this can be explained by the removal of a particle lying on top of it, which was possibly removed by the machining dynamics. For parameter 3, with a line energy of 2.67 J/m (Figure 5 right column), it is difficult to identify the position compared to the two previous parameters. The machining removed superficial particles and a significant ablation depth is obtained. This can

be seen well in the left area of the image, where a top layer particle is missing compared to the untreated image and no binder structures are visible in the exposed pore.

4. Conclusion

In the presented study, we investigated the modelling of a selective ablation process of electrodes on the basis of an anode. It was found that the model is applicable and gives good and comparable results to the experimental investigations. However, it was also found that the transfer from cathodes to anodes may require a more detailed definition of the energy propagation.

- The ablation thresholds agree well between model (0.63 J/m) and experiment (0.7 J/m).
- The depth effect of the selective ablation could be compared and differs in the range up to 2.75 J/m in the gradient only, which will be corrected in the next step by modifying the energy propagation.
- Two processing thresholds were found. From an energy per unit length of 0.67 J/m, the selective process begins without damaging the active material. The second process threshold is at 1.6 J/m, at which damage to the active material begins and thus the process window for a selective process is limited.

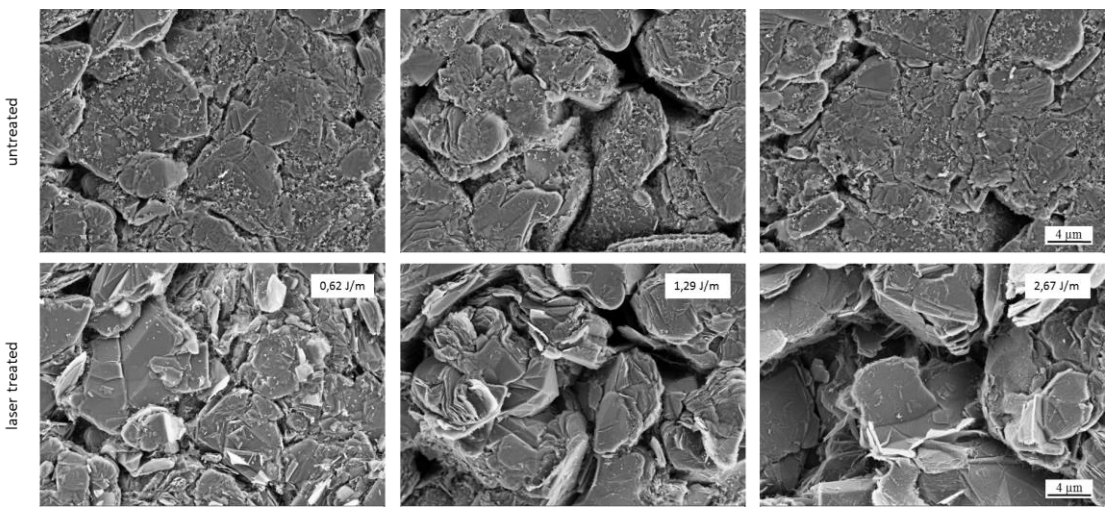

Fig. 5. Top-view SEM imaged of anodes before (upper) and after (lower) laser treatment with energies per unit length of 0.62 J/m (left), 1.29 J/m (middle) and 2.67 J/m (right)

Acknowledgements

The authors gratefully acknowledge the support of the German Federal Ministry of Economic Affairs and Energy by funding the project “structur.E—Strukturierte Anoden für verbesserte Schnellladefähigkeit und Steigerung der Energiedichte von Lithium-Ionenbatterien” (No. 03ETE018F).

References

Bolsinger, M., Weller, M., Ruck, S., Kaya, P., Riegel, H., Knoblauch, V., 2019, Selective surface treatment by means of IR-laser—A new approach to enhance the rate capability of cathodes for Li-ion batteries, Electrochim. Acta 330, 135163

Carslaw, H. S., Jaeger, J. C., Ingersoll, L. R., Zobel, O. J., Ingersoll, A. C. U., van Vleck, J. H., 1948, Conduction of Heat in Solids and Heat Conduction, Bd. 1 (Oxford University, New York)

Collishaw, P. G. , Evans, J. R. G., 1994, An assessment of expressions for the apparent thermal conductivity of cellular materials, J. Mater. Sci. 29, 486–498

Do, Truong, Shin, Changseop, Kwon, Patrick, Yeom, Junghoon, 2016, Fully-Enclosed Ceramic Micro-burners Using Fugitive Phase and Powder-based Processing, Scientific Reports 6, 31336

Enderle, S., Bolsinger, M., Ruck, S., Knoblauch, V., Riegel, H., 2020 Thermophysical modeling of selective laser ablation processing of lithium-ion battery cathodes, J. Laser Appl. 32, 042008

Pfleging, W., 2021, Recent progress in laser texturing of battery materials: a review of tuning electrochemical performances, related material development, and prospects for large-scale manufacturing, Int. J. Extem. Manuf. 3

Ruck, S., Bolsinger, M., Weller, M., Knoblauch, V., Riegel, H., 2019, Enhancing the rate capability of highly densified Li-Ion battery cathodes by selective laser ablation, Proc. SPIE 10906, 109061D

Schmidt, D., Kamlah M., Knoblauch, V., 2018, Highly densified NCM-cathodes for high energy Li-ion batteries: Microstructural evolution during densification and its influence on the performance of the electrodes, J. Energy Storage 17, p. 213–223

Smith, D. S., Alzina, A., Bourret, J., Nait-Ali, B., Pennec, F., Tessier-Doyen, N., Otsu, K., Matsubara, H., Elser, P., Gonzenbach, U. T., 2013, Thermal conductivity of porous materials, J. Mater. Res. 28, 2260–2272

Vadakkepatt, A., Trembacki, B., Mathur, S. R., Murthy, J. Y. 2016, Bruggeman's exponents for effective thermal conductivity of lithium-ion battery electrodes, J. Electrochem. Soc. 163, A119–A130

Weber, R., Graf, T., Berger, P., Onuseit, V., Wiedenmann, M., Freitag, C., Feuer, A., 2014, Heat accumulation during pulsed laser materials processing, Opt. Express 22, 11312–11324